CRACK PROBLEMS IN LARGE REINFORCED CONCRETE STRUCTURES SUBJECTED TO THERMAL LOADING

A. Carpinteri

Estratto da:

HEAT and TECHNOLOGY

CALORE e TECNOLOGIA

Volume 4 · No. 1 · 1986

Published quarterly by
PITAGORA EDITRICE BOLOGNA

HEAT and TECHNOLOGY
CALORE e TECNOLOGIA
Vol. 4 • No. 1 • 1986

CRACK PROBLEMS IN LARGE REINFORCED CONCRETE STRUCTURES SUBJECTED TO THERMAL LOADING

Alberto Carpinteri (*)

ABSTRACT

Damage is often highly localized in large reinforced concrete structures and a discrete cracking description is more realistic than a smeared one. A fracture mechanics methodology is proposed with the aim of reproducing crack growth, stiffness variation and loading evolution in redundant reinforced concrete members subjected to temperature gradients through the depth. By increasing temperature gradient, a brittle and rapid crack propagation or a ductile and slow crack growth may occur according to the stability conditions. Steel percentage, size scale and initial crack depth are demonstrated to be fundamental factors in such problems.

SOMMARIO

Nelle strutture in cemento armato di grandi dimensioni il danneggiamento meccanico è spesso altamente localizzato e un modello discreto della fessurazione risulta più realistico di uno continuo. Si propone un algoritmo di meccanica della frattura con lo scopo di descrivere la propagazione di fessure, le variazioni di rigidezza e l'evoluzione dei carichi negli elementi strutturali iperstatici di calcestruzzo armato soggetti a gradienti di temperatura attraverso lo spessore. Aumentando il gradiente di temperatura, possono manifestarsi una propagazione fragile e rapida o una crescita duttile e lenta della fessura in relazione alle condizioni di stabilità. La percentuale d'armatura, la scala dimensionale e la profondità iniziale della fessura si dimostrano essere fattori fondamentali.

(*) Istituto di Scienza delle Costruzioni, Università di Bologna, 40136 Bologna, Italy.

NOTATION

a	crack length
A	cross-section area
A_s	steel area
b	beam depth
d	crack distance from the fixed-end C
E	Young's modulus
F	reaction of reinforcement
F_P	force of reinforcement plastic flow
f_y	steel yield strength
h	distance of reinforcement from external surface
K_I	stress-intensity factor
K_{IC}	fracture toughness of concrete
I	moment of inertia
ℓ	beam length
M	bending moment
M_P	bending moment of reinforcement plastic flow
M_F	bending moment of crack propagation
M_S	bending moment after unstable crack propagation
M^f	fictitious bending moment
M^r	real bending moment
N_P	brittleness number $= (f_y b^{1/2}/K_{IC}) \cdot (A_s/A)$
r	ratio defined in eq. (7)
t	beam thickness
Y_M, Y_F	functions defined in ref. [4]
α	coefficient of thermal expansion of concrete
Δt	temperature gradient
$\lambda_{MM}, \lambda_{MF}$	crack compliances
ξ	crack depth $= a/b$
φ	local rotation
φ_F	rotation at crack propagation
φ^r	real rotation

1. INTRODUCTION.

Thermal loads on reinforced concrete structures are recognized to be dangerous, specially when nuclear power plant structures are considered. The ACI 349. 1R-80 report [1] presents a design-oriented approach to the problem of R.C. frames and axisymmetric shells. Smeared member cracking is assumed for purposes of obtaining the cracked structure thermal forces and moments. Two types of cracked members are analyzed: (1) end-cracked, and (2) interior-cracked. Obviously, the fix-end moments depend not only on the cracked length but also on the location of the cracked portion along the member as well as on the damage level, which is represented by a reduced moment of inertia of the damaged cross-section.

On the other hand, damage is often highly localized in large R.C. structures [2, 3] and a discrete cracking description would be much more realistic than a smeared one. In the present paper, a fracture mechanics methodology is proposed with the aim of reproducing crack growth, stiffness variations and loading evolutions in redundant R.C. members subjected to increasing temperature gradients through the depth.

An initial edge crack is assumed to produce local yielding of steel reinforcement and strain-hardening of bending moment vs. local rotation behaviour. By increasing temperature gradient, a brittle and rapid crack propagation condition or a ductile and slow crack growth condition is achieved, according to the stability conditions obtained in [4, 5]. Steel percentage and structural size scale are fundamental factors in this LEFM approach.

In small and medium-sized R.C. structures discrete cracking is always coupled with smeared damage and the strain energy density approach recently proposed by Carpinteri and Sih [6, 7] can simulate these cases more satisfactorily than the simple inertia-reduction approach proposed in [1]. This will be the object of future research.

2. BENDING MOMENT VS. LOCAL ROTATION CONSTITUTIVE LAW.

Let the cracked concrete beam element in Fig. 1 be subjected to the bending moment M and to an eccentric axial force F due to the statically undetermined reaction of the reinforcement. It is well-known that bending moment M* and axial force F* induce stress-intensity factors at the crack tip respectively equal to:

$$K_I^{(M)} = \frac{M^*}{b^{3/2}\,t}\,Y_M(\xi)\,, \tag{1-a}$$

$$K_I^{(F)} = \frac{F^*}{b^{1/2}\,t}\,Y_F(\xi)\,, \tag{1-b}$$

where Y_M and Y_F are given in [4].

On the other hand, M* and F* produce local rotations respectively equal to:

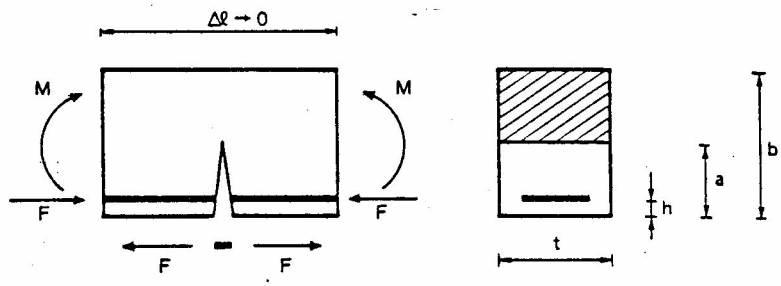

Fig. 1 - Cracked concrete beam element.

$$\varphi^{(M)} = \lambda_{MM} M^* , \tag{2-a}$$

$$\varphi^{(F)} = \lambda_{MF} F^* , \tag{2-b}$$

where:

$$\lambda_{MM} = \frac{2}{b^2 t E} \int_0^{\xi} Y_M^2(\xi)\, d\xi , \tag{3-a}$$

$$\lambda_{MF} = \frac{2}{b t E} \int_0^{\xi} Y_M(\xi)\, Y_F(\xi)\, d\xi . \tag{3-b}$$

Up to the moment of steel yielding or slippage, the local rotation in the cracked cross-section is equal to zero:

$$\varphi = \varphi^{(M)} + \varphi^{(F)} = 0. \tag{4}$$

Eq. (4) is the congruence condition giving the unknown force F. Recalling that (Fig. 1):

$$M^* = M - F\left(\frac{b}{2} - h\right), \tag{5-a}$$

$$F^* = -F , \tag{5-b}$$

eqs (2) and (4) provide:

$$\frac{Fb}{M} = \frac{1}{\left(\frac{1}{2} - \frac{h}{b}\right) + r(\xi)} , \tag{6}$$

where:

$$r(\xi) = \frac{\int_0^{\xi} Y_M(\xi)\, Y_F(\xi)\, d\xi}{\int_0^{\xi} Y_M^2(\xi)\, d\xi} . \tag{7}$$

If a perfectly plastic behaviour of the reinforcement is considered (yielding or slippage), from eq. (6) the moment of plastic flow for the reinforcement results:

$$M_P = F_P b \left[\left(\frac{1}{2} - \frac{h}{b} \right) + r(\xi) \right] . \tag{8}$$

However, it should be observed that, if concrete presents a low crushing strength and steel a high yield strength, crushing of concrete can precede plastic flow of reinforcement.

The mechanical behaviour of the cracked reinforced concrete beam section is rigid until the bending moment M_P is exceeded, i.e., $\varphi = 0$ for $M \leqslant M_P$. On the other hand, for $M > M_p$ the $M - \varphi$ diagram becomes linear hardening:

$$\varphi = \lambda_{MM} (M - M_P) . \tag{9}$$

After the plastic flow of reinforcement, the stress-intensity factor at the crack tip is given by the superposition principle:

$$K_I = K_I^{(M)} + K_I^{(F)} . \tag{10}$$

Recalling eqs (1) and considering the loadings:

$$M^* = M - F_P \left(\frac{b}{2} - h \right) , \tag{11-a}$$

$$F^* = - F_P , \tag{11-b}$$

the global stress-intensity factor results:

$$K_I = \frac{Y_M(\xi)}{b^{3/2} t} \left[M - F_P \left(\frac{b}{2} - h \right) \right] - \frac{F_P}{b^{1/2} t} Y_F(\xi) . \tag{12}$$

The moment of crack propagation is then:

$$\frac{M_F}{K_{IC} b^{3/2} t} = \frac{1}{Y_M(\xi)} + N_P \left[\frac{Y_F(\xi)}{Y_M(\xi)} + \frac{1}{2} - \frac{h}{b} \right] , \tag{13}$$

with:

$$N_P = \frac{f_y b^{1/2}}{K_{IC}} \cdot \frac{A_s}{A} , \tag{14}$$

while the rotation at crack propagation is:

$$\varphi_F = \lambda_{MM} (M_F - M_P) . \tag{15}$$

The crack propagation moment is plotted in Fig. 2 as a function of the crack depth ξ and varying the brittleness number N_P. For low N_P values, i.e., for low reinforced beams or for small cross-sections, the fracture moment decreases while the crack extends, and a

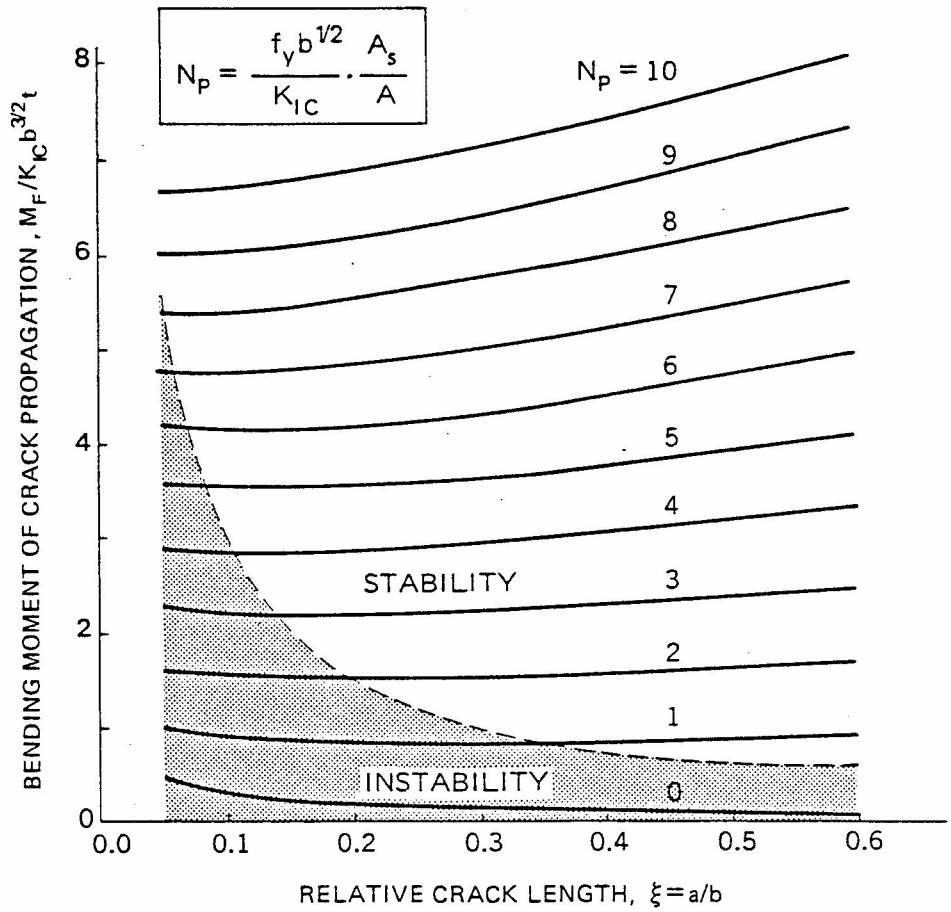

Fig. 2 - Crack propagation moment against relative crack length.

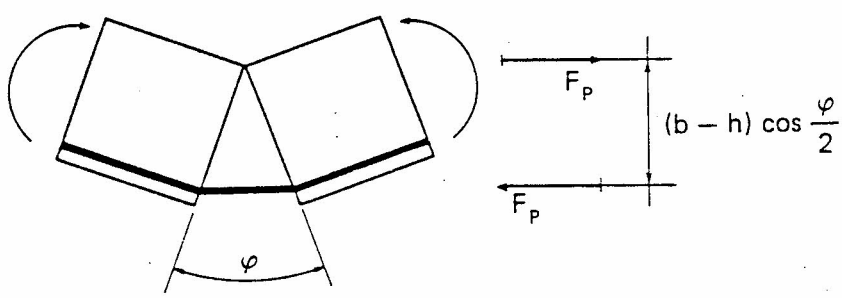

Fig. 3 - Statical scheme of complete disconnection of concrete.

typical phenomenon of unstable fracture occurs. For $N_P \geqslant 0.7$, a stable branch follows the unstable one, while for $N_P \geqslant 8.5$ only the stable branch remains. The locus of the minima is represented by a dashed line in Fig. 2. In the upper zone the fracture process in stable whereas it is unstable in the lower one.

Rigid behaviour ($0 \leqslant M \leqslant M_P$) is followed by linear hardening ($M_P < M < M_F$). The latter stops when crack propagation occurs. If the fracture process in unstable, diagram $M - \varphi$ presents a discontinuity and drops from M_F to $F_P b$ with a negative jump. In fact, in this case a complete and instantaneous disconnection of concrete occurs. The new moment $F_P b$ can be estimated according to the scheme of Fig. 3. The non-linear descending law:

$$M = F_P(b - h) \cos \frac{\varphi}{2} , \tag{16}$$

is thus approximated by the perfectly plastic one:

$$M = M_S = F_P b . \tag{17}$$

On the other hand, if the fracture process is stable, diagram $M - \varphi$ does not present any discontinuity and, after the linear hardening stage, goes on with the perfectly plastic law [4]:

$$M = M_F . \tag{18}$$

3. VIRTUAL WORK PRINCIPLE APPLIED TO LOCALLY CRACKED REDUNDANT STRUCTURES.

Let us consider the doubly fixed-end R.C. beam in Fig. 4-a, cracked in section B and subjected to the linear temperature gradient $2\Delta T/b$. The redundant system is reduced to the isostatic scheme in Fig. 4-b, which is considered as the superposition of the two fictitious partial schemes in Figs 4-c and d.

The application of Virtual Work Principle to the fictitious schemes gives:

$$\int_S \frac{M_i^f M^r}{EI} ds + \int_S M_i^f \left(\frac{d\varphi}{ds}\right) ds + M_i^f(B)\, \varphi^r(B) = 0, \quad \text{for} \quad i = 1, 2 , \tag{19}$$

where the first integral is the work of the fictitious bending moments over the real elastic rotations, the second integral is the contribution of the thermal rotations, while the last is the work of the fictitious moment in section B over the real elastic rotation in section B.

When it is $M^r(B) \leqslant M_P$ the rotation in B is zero, $\varphi^r(B) = 0$, and the last term is missing in eq. (19). When $M_P < M^r(B) < M_F$ (hardening stage), eq. (19) is valid and the real elastic rotation in section B can be expressed as follows:

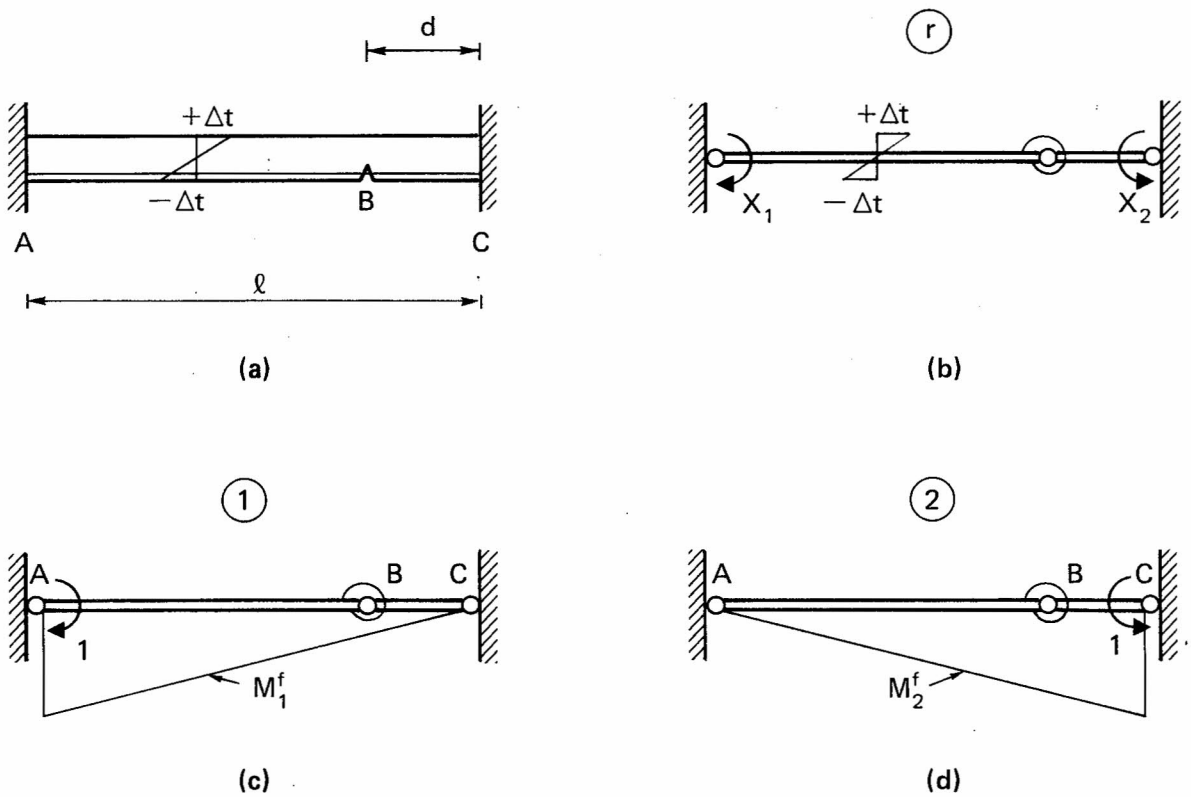

Fig. 4 - Doubly fixed-end reinforced concrete beam (a); isostatic scheme (b); fictitious partial schemes (c, d).

$$\varphi^r(B) = \lambda_{MM}[M^r(B) - M_P]\,. \tag{20}$$

Eventually, when $\varphi^r(B) \geqslant \varphi_F$ we have $M^r(B) = M_S$, the hinge B becomes perfectly plastic, and the term $\varphi^r(B)$ in eq. (19) is undetermined. It is then necessary to resort to the scheme in Fig. 5, where the statically undetermined shear force in B is equal to:

$$X = \frac{3\left(\dfrac{EI\,\alpha\,\Delta t}{b} - \dfrac{M_S}{2}\right)[d^2 - (\ell - d)^2]}{[d^3 + (\ell - d)^3]}\,. \tag{21}$$

The real rotation in section B is given by the addition of the end rotations of the cantilever beams in Fig. 5:

$$\varphi^r(B) = \varphi_1^r(B) + \varphi_2^r(B)\,, \tag{22}$$

with:

$$\varphi_1^r(B) = \frac{2\alpha\,\Delta t}{b}(\ell - d) - \frac{M_S(\ell - d)}{EI} + \frac{X(\ell - d)^2}{2EI}\,, \tag{23-a}$$

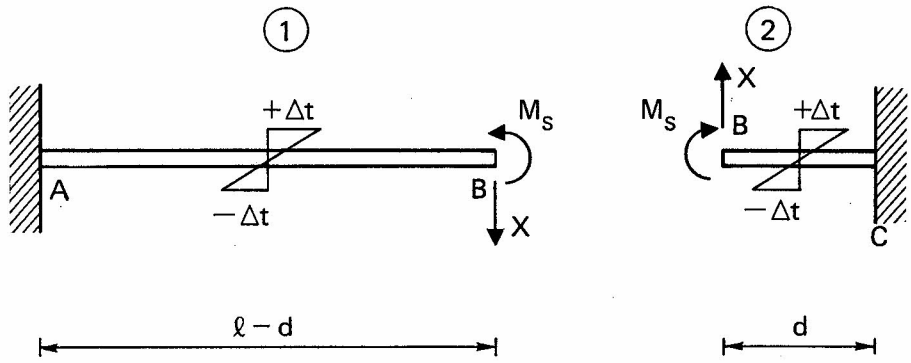

Fig. 5 – Internal reactions at the fracture limit condition.

$$\varphi_2^I(B) = \frac{2\alpha\Delta t}{b}\, d - \frac{M_S d}{EI} - \frac{Xd^2}{2EI}. \tag{23-b}$$

Eqs. (19) provide a system of linear algebraical equations where the unknowns terms are the fixed-end bending moments X_i, $i = 1, 2$;

$$aX_1 + bX_2 = p, \tag{24-a}$$

$$bX_1 + cX_2 = q, \tag{24-b}$$

with:

$$a = \frac{\ell}{3EI} + \lambda_{MM}\left(\frac{d}{\ell}\right)^2, \tag{25-a}$$

$$b = \frac{\ell}{6EI} + \lambda_{MM}\left(\frac{d}{\ell}\right)\left(1 - \frac{d}{\ell}\right), \tag{25-b}$$

$$c = \frac{\ell}{3EI} + \lambda_{MM}\left(1 - \frac{d}{\ell}\right)^2, \tag{25-c}$$

$$p = -\frac{\alpha\Delta t\ell}{b} + \lambda_{MM} M_P \frac{d}{\ell}, \tag{25-d}$$

$$q = -\frac{\alpha\Delta t\ell}{b} + \lambda_{MM} M_P \left(1 - \frac{d}{\ell}\right). \tag{25-e}$$

If we assume an increasing temperature gradient ΔT, the behaviour of the cracked section

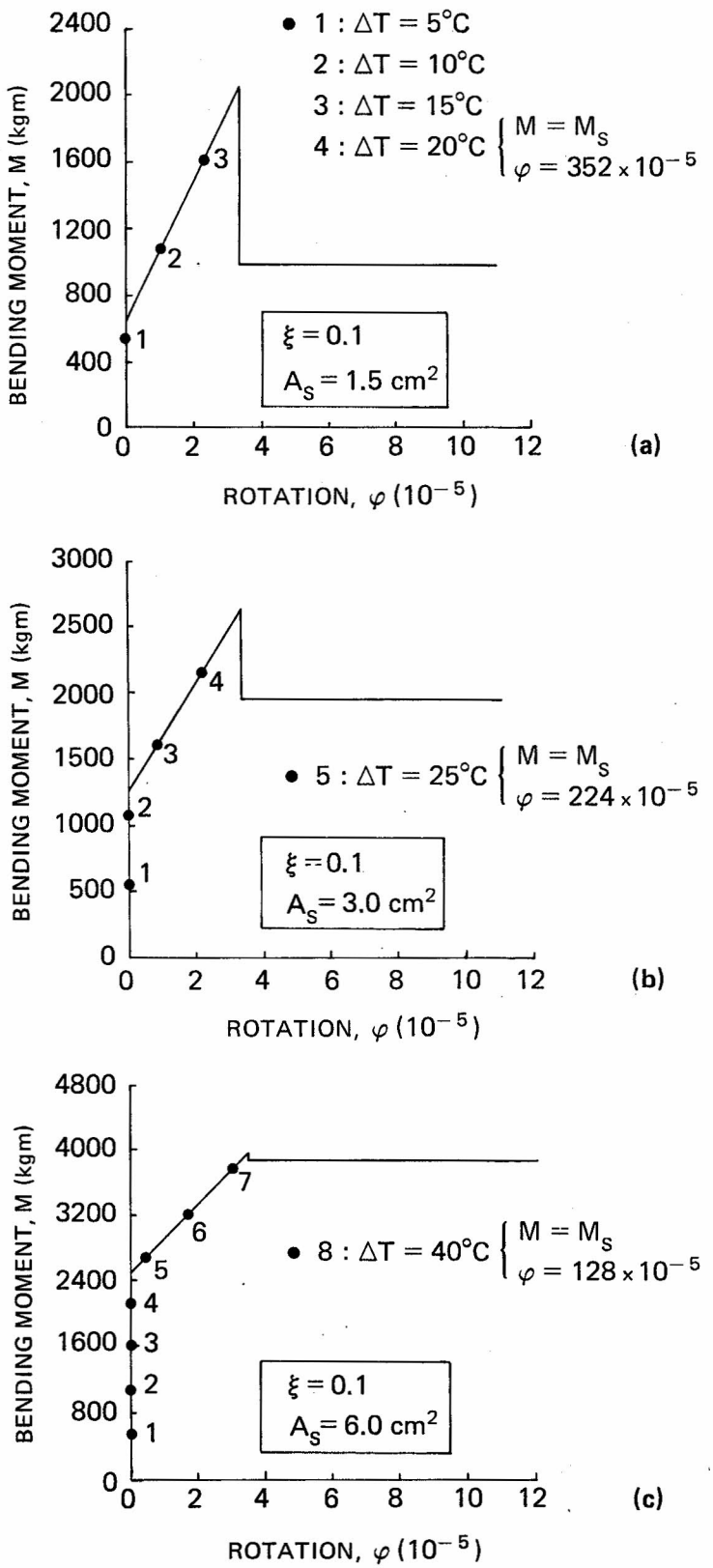

Fig. 6 - Bending moment against local rotation in the cracked cross section (shallow crack, $\xi = 0.1$).

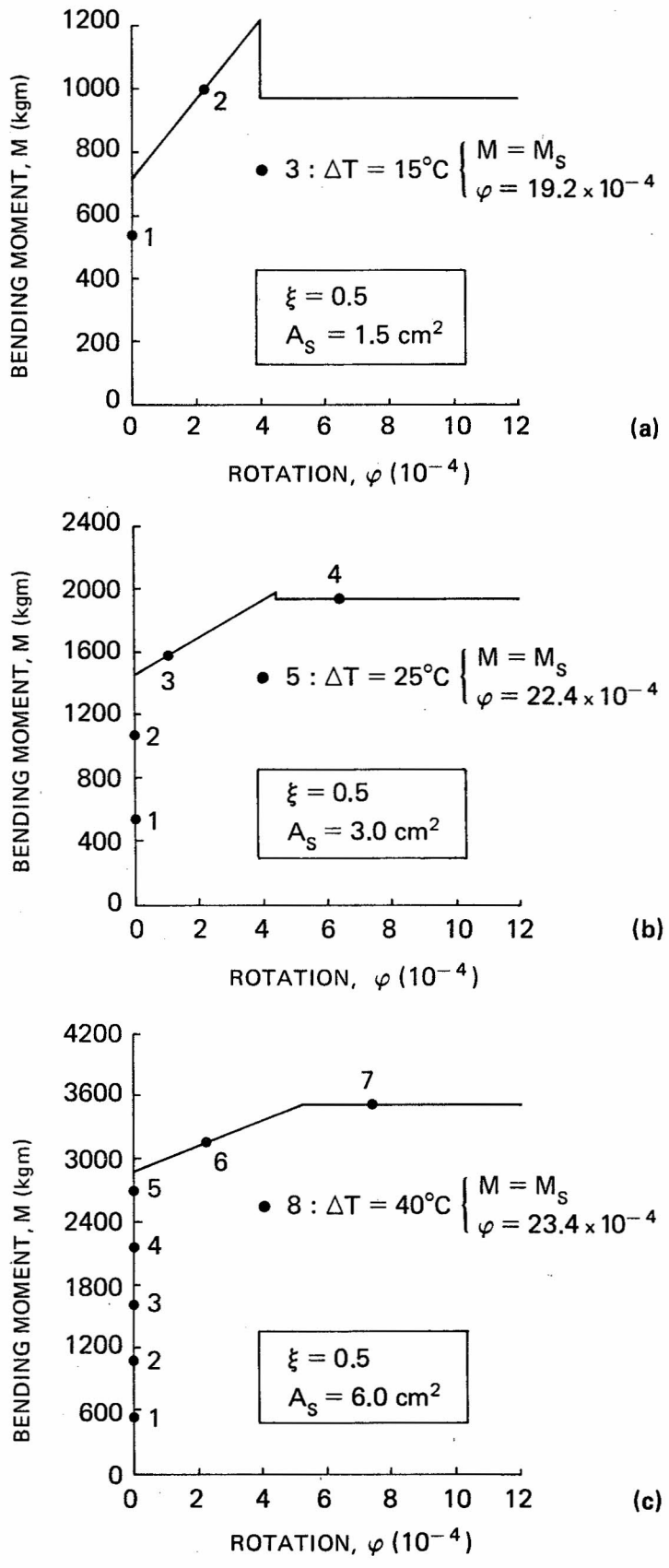

Fig. 7 - Bending moment against local rotation in the cracked cross section (deep crack, $\xi = 0.5$).

B is rigid at the beginning and the value $\lambda_{MM} = 0$ is to be inserted into eqs (25). Then, for $M_P < M^r(B) < M_F$, the behaviour becomes linear hardening and the compliance given in eq. (3-a) is to be considered in eqs (25). Eventually, for $\varphi^r(B) \geqslant \varphi_F$ the perfect plastic flow of section B is bounded by the stiffness of the remaining part of the structure and eqs (21), (22) and (23) are to be applied.

4. DISCUSSION.

Some numerical examples are presented with regard to the doubly fixed-end R.C. beam in Fig. 4-a. The following geometrical and mechanical properties are assumed: $\ell = 400$ cm, $b = 30$ cm, $t = 20$ cm, $E = 300{,}000$ kg/cm^2, $I = 45{,}000$ cm^4, $d = 200$ cm, $\alpha = 0.000012\,°C^{-1}$, $f_y = 2400$ kg/cm^2, $h = 3$ cm, $K_{IC} = 150$ kg/cm$^{3/2}$. The influence of steel area A_s and initial crack depth ξ is investigated.

The diagrams in Fig. 6-a, b and c represent the bending moment versus local rotation in the cracked cross-section B (Fig. 4-a) for $\xi = 0.1$ (shallow crack) and respectively when $A_s = 1.5, 3.0, 6.0$ cm^2. The moment of reinforcement plastic flow increases by increasing the steel area, while the hardening slope depends only on the initial crack depth. The moment of crack propagation increases by increasing the steel area as well as the post-collapse bending moment $M_S = F_p b$. On the other hand, the negative jump at crack instability decreases when more reinforced beams are treated. We observe that such a discontinuity nearly disappears when $A_s = 6.0$ cm^2. For $A_s > 6.0$ cm^2, the crack growth becomes slow and stable according to the diagrams in Fig. 2. In fact, for intermediate N_P numbers ($0.7 \lesssim N_P \lesssim 4.0$), the crack may present an initial unstable propagation and then stop when the ascending branch of the curve N_P = constant is achieved. For high N_P numbers ($N_P \gtrsim 4.0$) the crack growth is only slow and stable so that the hardening behaviour with small slope can be approximated by the plastic limit $M = M_S = M_F$.

The $M - \varphi$ values related to the increasing temperature gradients are reported in Fig. 6. Of course, the fracture collapse is achieved for lower gradients when the beam is weak reinforced. For example, for $A_s = 1.5$ cm^2 the fracture propagation occurs when $\Delta T = 19\,°C$, whereas for $A_s = 6.0$ cm^2 it does when $\Delta T = 36.5\,°C$. Observe that, after the unstable crack growth in concrete, the local rotation in section B attains substantially higher values than during the hardening stage.

The diagrams in Fig. 7-a, b and c represent the bending moment versus local rotation for $\xi = 0.5$ (deep crack) and respectively when $A_s = 1.5, 3.0, 6.0$ cm^2. The trends are the same as in the preceding case. On the other hand, the fracture behaviour appears to be more stable, in agreement with the curves in Fig. 2, where $A_s = 6.0$ cm^2 provides the britteness number $N_P = 0.87$ and produces a stable behaviour for $\xi = 0.5$. Observe that, after the crack instability, the rotation is not much higher than before and that the variation in mechanical behaviour is not so sharp as it appears for $\xi = 0.1$ (Fig. 6).

ACKNOWLEDGMENTS

The author gratefully acknowledges the research support of "Ministero Pubblica Istruzione" and "Consiglio Nazionale delle Ricerche".

REFERENCES

[1] ACI 349.1R-80: *Reinforced Concrete Design for Thermal Effects on Nuclear Power Plant Structures,* American Concrete Institute (1980).

[2] A. Carpinteri: Static and energetic fracture parameters for rocks and concrete, *Materials and Structures,* R.I.L.E.M., Vol. 14, pp. 151-162 (1981).

[3] A. Carpinteri: Application of fracture mechanics to concrete structures, *Journal of the Structural Division,* American Society of Civil Engineers, Vol. 108, pp. 833-848 (1982).

[4] A. Carpinteri: Stability of fracturing process in R.C. beams, *Journal of Structural Engineering,* American Society of Civil Engineers, Vol. 110, pp. 544-558 (1984).

[5] Al. Carpinteri, An. Carpinteri: Hysteretic behaviour of R.C. beams, *Journal of Structural Engineering,* American Society of Civil Engineers, Vol. 110, pp. 2073-2084 (1984).

[6] A. Carpinteri, G.C. Sih: Damage accumulation and crack growth in bilinear materials with softening: application of strain energy density theory, *Theoretical and Applied Fracture Mechanics,* Vol. 1, pp. 145-159 (1984).

[7] G.C. Sih: Mechanics of material damage in concrete, *Fracture Mechanics of Concrete: Material Characterization and Testing,* Edited by A. Carpinteri and A.R. Ingraffea, Martinus Nijhoff Publishers, pp. 1-29 (1984).